Journal of Chemical&Engineering Data

pubs.acs.org/jced Article

Isobaric Vapor−Liquid Equilibrium of the Azeotropic Mixture *n*-Hexane + Ethanol with 1-Butylpyrrolidin-2-one as a Greener Entrainer and 1-Methylpyrrolidin-2-one as a Benchmark Entrainer

Published as part of Journal of Chemical & Engineering Data special issue "In Honor of Tejraj M. Aminabhavi".

Dhoni Hartanto,* Boelo Schuur, Anton A. Kiss, and André B. de Haan

Cite This: *J. Chem. Eng. Data* 2025, 70, 4091−4104 Read Online

ACCESS | Metrics & More | Article Recommendations | Supporting Information

ABSTRACT: Green solvents have emerged as promising green entrainers to substitute conventional entrainers in extractive distillation to separate azeotropic mixtures. However, the limited availability of thermodynamic data for green-solvent-containing mixtures continues to hinder their practical implementation in this process. This study is the first to report experimental vapor−liquid equilibrium (VLE) data for the *n*-hexane + ethanol azeotropic system containing the greener entrainer 1-butylpyrrolidin-2-one (NBP) alongside the benchmark entrainer 1-methylpyrrolidin-2-one (NMP). Using a Fischer Labodest VLE602 ebulliometer, VLE measurements were performed at pressures of 50.0 and 100.0 kPa and various entrainer-to-feed ratios (E/F). The reliability of the reported VLE data was tested and confirmed using the Van Ness thermodynamic consistency test. The results show that NBP enhances relative volatility and effectively eliminates the azeotrope, performing comparably to the benchmark entrainer NMP. The nonrandom-two-liquid (NRTL) model was utilized to regress the investigated VLE data and determine the optimum binary interaction parameters (BIPs). As a result, the NRTL model demonstrates good agreement with the experimental data. This thermodynamic modeling confirms the data's reliability and suitability for process design, highlighting NBP's potential as an environmentally friendly alternative entrainer in extractive distillation.

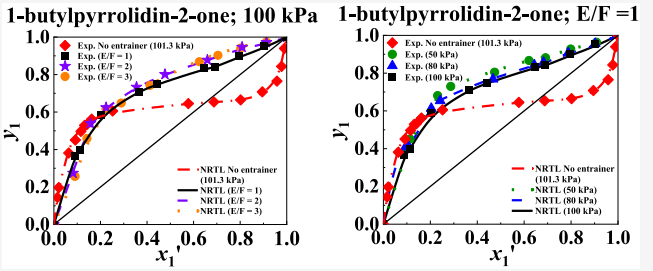

1. INTRODUCTION

In the process industry, separation processes are among the most energy-intensive and technically challenging operations, accounting for over half of the total energy and costs.[1,2] A primary challenge in these processes arises from the azeotropic behavior of the mixtures. Azeotropes are characterized by identical compositions in the vapor and liquid phase at specific temperatures and pressures, resulting from strong nonideal intermolecular interactions. This behavior makes the mixture difficult to separate. One such azeotropic system of interest is the *n*-hexane−ethanol mixture, which appears across various industries. The mixture of alkane-alcohol, such as *n*-hexane and ethanol, often coexists in various petrochemical processes.[3] Low-carbon alcohols, such as ethanol, can be produced from syngas, which is derived from the gasification of coal or natural gas.[4] In this direct conversion of syngas to ethanol, C_{2+} hydrocarbons, such as *n*-hexane, are formed alongside ethanol.[5] Additionally, in the Fischer−Tropsch synthesis, the oxygenated products such as ethanol can coexist with hydrocarbons, including *n*-hexane, as both are generated during the process.[6] As both components are widely used solvents in numerous industries,[7] it is crucial to effectively separate this mixture in order to obtain high-purity *n*-hexane and ethanol, despite the azeotropic behavior present in the mixture.

The most employed separation method is distillation technology, which is valued for its versatility in handling broad feed flow rates and compositions. It is also suitable for separating complex mixtures on a larger scale across various applications to achieve high-purity components.[8,9] Globally, distillation is utilized in over 100,000 active columns, contributing to more than half of the total capital and operational costs in the chemical processing facilities.[10] However, conventional distillation is limited when dealing with azeotropic systems. To overcome these limitations, advanced distillation technologies such as extractive distillation are required to achieve a successful azeotropic separation. This

Received: June 29, 2025
Revised: August 25, 2025
Accepted: August 26, 2025
Published: September 10, 2025

Table 1. Technical Information of the Chemicals

chemicals	CAS no.	molecular weight (g/mol)	boiling point (K)[a,b]	density (g/cm^3)[a,c]	commercial suppliers	purity (in a mass fraction)[a]	analysis method	purification
n-hexane	110-54-3	86.18	342.15	0.660	Merck	≥0.990	GC[d]	none
ethanol	64-17-5	46.07	351.44	0.790	Merck	≥0.999	GC[d]	none
1-butylpyrrolidin-2-one	3470-98-2	141.21	514.15	0.960	BioPSX	0.995	GC[d]	none
1-methylpyrrolidin-2-one	872-50-4	99.13	475.15	1.028	Sigma-Aldrich	≥0.995	GC[d]	none
acetone	67-64-1	58.08	329.15	0.791	Merck	≥0.998	GC[d]	none

[a]Specified by the commercial suppliers. [b]At a pressure of 101.3 kPa. [c]At a temperature of 298.15 and a pressure of 101.3 kPa. [d]Gas chromatography (GC)

technology involves the introduction of a high-boiling and thermally stable entrainer to enhance the relative volatility of the key component. This enables separation beyond the azeotropic constraints and contributes to reduced energy and water usage, costs, and CO_2 emissions.

Considering its potential, the sustainability of extractive distillation is undermined by the widespread use of conventional entrainers, such as 1-methylpyrrolidin-2-one (NMP). These solvents are known to be toxic and non-eco-friendly. Regulatory bodies including E.U. REACH and the U.S. EPA are progressively imposing restrictions on such substances due to health and environmental concerns.[11,12] Consequently, there is a growing demand for alternative entrainers that combine separation efficacy with environmental compatibility.

Despite the increasing interest in green solvents, 1-butylpyrrolidin-2-one (NBP), also known commercially as TamiSolve NxG, is a promising yet underexplored greener solvent. Furthermore, the experimental VLE data and the binary interaction parameters (BIPs) for *n*-hexane + ethanol with NBP remain unavailable, limiting process design. This study addresses this gap.

Recent studies have explored green solvents as potential entrainers for various azeotropic or close boiling mixtures in extractive distillation, such as deep eutectic solvents (DESs), including natural deep eutectic solvents (NADESs),[12−18] biological buffers,[19] ionic liquids (ILs),[20−25] and biobased solvents.[26−32] In the separation of *n*-hexane−ethanol, current research has reported several potential entrainers, particularly focusing on the VLE data for the binary mixture of *n*-hexane with butyl propanoate and butyl butanoate, respectively,[33] along with VLE data for the binary mixture of ethanol with butyl propanoate and butyl butanoate.[34] In these studies, however, only binary VLE data were provided and no VLE data were provided for the pseudo-ternary mixture of *n*-hexane−ethanol containing butyl propanoate and butyl butanoate as entrainers. In addition, ionic liquids, including cations such as 1-ethyl-3-methyl-imidazolium [EMIM], 1-butyl-3-methyl-imidazolium [BMIM], and 1-hexyl-3-methyl-imidazolium [HMIM] combined with hydrogen sulfate [HSO_4], have been studied for *n*-hexane−ethanol separation.[35] Furthermore, the high cost of ionic liquids compared with conventional solvents poses challenges for their industrial application. Extractive distillation experiments using a simple round-bottom flask have also been reported using deep eutectic solvents (DESs), such as choline chloride−glycerol, menthol−decanoic acid, and menthol−dodecanoic acid.[36] However, choline chloride−glycerol-based DES faces miscibility issues, and the maximum purity of *n*-hexane obtained using these DESs with a mass fraction of 0.05 was only 0.87 mass fraction. Additionally, Wang et al. investigated the impact of conventional solvents such as dimethyl sulfoxide, 1,2-propanediol, 1,3-propanediol, ethylene glycol, dimethylformamide, dimethylacetamide, and NMP on the relative volatility of *n*-hexane−ethanol mixture.[37] This publication provided only predicted results without the complete experimental VLE data.

According to the prediction results using unimolecular quantum chemical calculation and group contribution methods from our previous work, NBP demonstrated a comparable relative volatility to NMP.[15] Furthermore, NBP is classified by the European Chemical Agency as a nontoxic and non-reprotoxic solvent, making it a safer alternative to conventional solvents.[38] In contrast, NMP is deemed as a toxic chemical. The No Observed Adverse Effect Level (NOAEL) for developmental toxicity exceeds 500 mg/kg body weight/day for NBP, in contrast to 160 mg/kg body weight/day for NMP.[39,40] As NOAEL values define the maximum dose at which there are no harmful effects on fetal development. A higher NOAEL indicates a lower toxicity. This suggests that NBP has lower fetal development toxicity than NMP. In addition, NBP complies with the principles of green chemistry by employing biobased and economically viable glutamic acid as a renewable feedstock. Its synthesis pathway minimizes environmental impact by generating near-zero waste throughout the process.[41]

From a technical standpoint, NBP possesses a high boiling point (514.15 K at a pressure of 101.3 kPa), which is higher than NMP (475.15 K at a pressure of 101.3 kPa), favorable thermal stability, and good polarity (Hansen solubility parameters, (δ_P) = 8.2 MPa$^{1/2}$, which is comparable to those of NMP with δ_P = 12.3 MPa$^{1/2}$). Additionally, NBP has a lower vapor pressure of 0.013 kPa at a temperature of 298.15 K, compared to NMP's vapor pressure of 0.044 kPa at the same temperature. These properties are advantageous for use in extractive distillation.[42−45]

Therefore, the present study evaluates for the first time the performance of NBP as a greener entrainer for separating the azeotropic mixture *n*-hexane−ethanol by measuring the VLE data for the *n*-hexane−ethanol mixture containing NBP. For comparative purposes, the VLE data for *n*-hexane−ethanol mixture in the presence of NMP as a benchmark entrainer was measured as NMP has been proven effective in commercial separation processes, offers less expensive solvent, and possesses good solvency properties, including high polarity and thermal stability.[46] NMP is already produced on a large scale. According to the European Chemical Agency, the production and import of NMP in Europe is from 10,000 to 100,000 tons per year.[47] This indicates that, despite some restrictions, NMP remains widely used in various industrial applications, such as lithium battery industries, membrane fabrication, pharmaceutical industries, and coal and oil exploration.[46] Furthermore, NMP is commonly employed in

https://doi.org/10.1021/acs.jced.5c00445
J. Chem. Eng. Data 2025, 70, 4091−4104

process separation, particularly as an entrainer in extractive distillation.[48−50]

The VLE data were tested for thermodynamic consistency using the Van Ness method.[51] To further assess the applicability of NBP, the nonrandom-two-liquid (NRTL) activity coefficient model was employed to regress the experimental data and determine optimum BIPs.[52] Accurate experimental VLE data and optimum BIPs obtained from thermodynamic modeling serve as critical foundations for the effective design and optimization of extractive distillation processes.

2. EXPERIMENTAL METHODS

The following sections outline the chemical information, the experimental setup and procedures, and the analytical methods employed.

2.1. Chemicals. The chemicals used in this work were procured from commercial suppliers. Their purity was assessed by using gas chromatography (GC). All chemicals were employed in their original state without any additional purification processes, as no significant contaminants were identified. Table 1 presents the detailed information on the chemicals used.

2.2. Experimental Setup and Procedures. Vapor−liquid equilibrium data for the binary system of *n*-hexane and ethanol, as well as for a pseudo-ternary mixture in the presence of 1-butylpyrrolidin-2-one and 1-methylpyrrolidin-2-one as entrainers, were measured using a Fischer Labodest VLE602 ebulliometer, Germany. According to the manufacturer's specifications, the measurement uncertainties for temperature and pressure are within ±0.01 K and ±0.01 kPa, respectively. Temperature measurements were performed by using a built-in thermocouple integrated into the ebulliometer. The schematic diagram of the experimental setup was provided by Dias et al.[53]

The mixtures and entrainers were accurately prepared using a Mettler Toledo AE200 analytical balance (USA) with an uncertainty of 0.0001 g. For each experimental run, approximately 100 mL of the prepared mixture was introduced into the ebulliometer to ensure a consistent liquid and vapor phase circulation in the setup. Vacuum conditions were established in a closed system using a Pfeiffer DUO 3 vacuum pump (Germany) and maintained with a Burkert 2871 pressure controller (Germany), integrated with the i-Fischer Unicontrol VLE digital interface. The targeted pressure was set and kept constant throughout the experiment. To ensure airtightness during the experiment, all sampling ports and vent outlets were sealed with caps fitted with silicone rubber septa and needle-valve stopcocks to prevent contamination from atmospheric pressure. Equilibrium conditions were achieved when the temperature and the pressure in the setup remained constant, within tolerances of 0.4 K and 0.1 kPa, respectively. The temperature stabilized after 30 min, and an additional 30 min was allowed before sampling to ensure that the equilibrium conditions were fully established. Therefore, the total duration of the experiment was 60 min. To maintain proper heating and temperature uniformity throughout the system, the setup utilized a heating rod immersed in the liquid chamber and a heating mantle surrounding the vapor chamber. Thermal insulation was applied to minimize heat loss from the setup. Simultaneously, continuous agitation was supplied by a magnetic stirrer to ensure thorough mixing of the liquid mixture. Additionally, the vapor generated during boiling was condensed and returned to the liquid mixture chamber as reflux, further enhancing internal circulation and thermal homogeneity. These methods ensured a stable and uniform temperature within the system during the experiment.

At equilibrium, around 0.1 mL of both the liquid phase and condensed vapor phase was sampled. Liquid samples were collected via a sampling valve, and vapor samples were obtained via syringe collection of condensed droplets. Each sample was immediately diluted in 1 mL of analytical-grade acetone, followed by GC analysis to determine the composition of the samples. This experimental approach aligns with established methodologies reported in previous studies.[26−28,54]

2.3. Analytical Methods. The composition analysis of the vapor and liquid phase samples was performed using a Thermo Scientific Trace 1300 GC (Switzerland), fitted with dual parallel ovens and an autosampler TriPlus 100 Liquid Samples. An Agilent DB-1MS capillary column (60 m length, 0.25 mm diameter, and 0.25 μm film thickness) was employed for component separation. The injection system operated in Split/Splitless (SSL) mode with a 1 μL injection volume. A temperature ramp was carried out in a multistep mode: starting at 30 °C, followed by the temperature increased at 10 °C/min to 45 °C, 5 °C/min to 60 °C, 2.5 °C/min to 80 °C, and 5 °C/min to 95 °C. A final rapid ramp of 50 °C/min brought the temperature to 320 °C, with the full temperature ramp lasting approximately 21 min. Detection was achieved using a flame ionization detector (FID) maintained at a temperature of 440 °C. The system operated with a helium carrier gas at 213.2 kPa, a column flow rate of 2 mL/min, a split flow of 300 mL/min (split ratio 150), an auxiliary hydrogen flow of 50 mL/min, a helium makeup flow of 40 mL/min, and an air flow of 350 mL/min.

Prior to sample analysis, calibration was performed using standard mixtures of known compositions for each component. The area fractions obtained from GC analysis were plotted against its corresponding mole fractions in the standard to construct a calibration curve. The mole fractions of components in the unknown sample were determined by applying their GC area fractions to the regression equation derived from the calibration curve. Each sample was analyzed in triplicate to minimize the analytical variation. The final composition values were determined as the average of the three analysis results. Expanded combined uncertainties for liquid and vapor composition, pressure, and temperature were calculated in accordance with the NIST technical note and JCGM guideline,[55,56] as detailed in eqs S1−S6 of the Supporting Information. The uncertainty values are reported alongside the VLE data in Section 3.1. In addition, the expanded combined uncertainties for vapor pressure measurements for *n*-hexane and ethanol were calculated using eqs S7 and S8, and are presented in Table S1 of the Supporting Information.

For verification of the chemical purity, an Agilent DB-Wax capillary column was employed. This column had a length of 60 m, a diameter of 0.25 mm, and a film thickness of 0.25 μm. A 1 μL injection volume was utilized. A temperature ramp was applied, starting at 30 °C. The temperature was initially increased at 10 °C/min to 90 °C, followed by a 5 °C/min to 95 °C. Subsequently, the temperature was elevated at 25 °C/min to 200 °C, and then further increased at 50 °C/min to a final temperature of 250 °C. Detection was carried out using a thermal conductivity detector (TCD) maintained at 200 °C,

https://doi.org/10.1021/acs.jced.5c00445
J. Chem. Eng. Data 2025, 70, 4091−4104

with helium serving as the carrier gas at a pressure of 213.2 kPa and a flow rate of 2 mL/min.

3. RESULTS AND DISCUSSION

3.1. Experimental Results. In this study, isobaric VLE data for the binary mixture of *n*-hexane and ethanol at 101.3 kPa were measured. The results of the VLE data are presented in Table 2. The liquid phase and vapor phase mole fractions of *n*-hexane are denoted as x_1 and y_1, respectively. While the equilibrium temperature is represented as T, and the activity coefficients for *n*-hexane and ethanol are indicated as γ_1 and γ_2, respectively. Additionally, the relative volatility of *n*-hexane to ethanol is denoted as α_{12}.

Table 2. VLE Data for Hexane (1) + Ethanol (2) at 101.3 kPa[a,b]

T/K	x_1	y_1	γ_1	γ_2	α_{12}
351.55	0.000	0.000		1.000	
347.18	0.015	0.144	8.161	1.031	11.05
345.39	0.021	0.197	8.490	1.046	11.53
340.46	0.064	0.381	6.248	1.035	9.05
338.61	0.092	0.451	5.416	1.026	8.08
336.82	0.116	0.497	5.025	1.043	7.52
335.90	0.132	0.529	4.847	1.035	7.39
335.35	0.141	0.548	4.790	1.028	7.40
334.26	0.162	0.567	4.461	1.060	6.77
332.51	0.252	0.606	3.247	1.169	4.56
331.39	0.577	0.645	1.568	1.958	1.33
331.26	0.687	0.654	1.341	2.597	0.86
331.52	0.802	0.665	1.159	3.922	0.49
332.35	0.895	0.708	1.075	6.218	0.28
334.07	0.958	0.765	1.025	11.598	0.14
336.10	0.978	0.843	1.036	13.378	0.12
339.32	0.990	0.939	1.028	10.275	0.15
342.15	1.000	1.000	1.000		

[a] T: equilibrium temperature; x_1 and y_1: mole fraction of *n*-hexane in the liquid and vapor phases, respectively; γ_1 and γ_2: activity coefficient of *n*-hexane and ethanol, respectively; α_{12}: relative volatility of *n*-hexane to ethanol. [b] Expanded combined uncertainties (U with $k = 2$): $U(T) = 0.20$ K, $U(P) = 0.20$ kPa, and $U(x_1) = U(y_1) = 0.006$.

To quantify the deviation from ideal solution behavior, eq 1 was used to determine the activity coefficient of component i in the binary mixture (γ_i).

$$\gamma_i = \frac{y_i P}{x_i P_i^{\text{sat}}} \tag{1}$$

For component i, the liquid phase mole fraction is denoted as x_i, while the vapor phase mole fraction is defined as y_i. The total pressure of the system and saturated vapor pressure of component i are expressed as P and P_i^{sat}, respectively. The constant of the extended Antoine and its equation retrieved from the physical properties databank of the Aspen Plus, is provided in Table 3 and was utilized to calculate the saturated vapor pressure for component i. As the VLE data measurements for the binary mixture were conducted at atmospheric and lower pressures, ideal gas behavior was assumed.

The relative volatility for the binary mixture of *n*-hexane (1) and ethanol (2) (α_{12}) is expressed in eq 2:

$$\alpha_{12} = \frac{y_1/x_1}{y_2/x_2} \tag{2}$$

To validate our method and setup, we compared the VLE data for the binary mixture of *n*-hexane and ethanol measured at 101.3 kPa from our work with the data from the existing literature. The T–x_1–y_1 diagram, as illustrated in Figure 1, and the x_1–y_1 diagram, as shown in Figure S1 of the Supporting Information, show that our VLE data are consistent with those reported by Sinor and Weber,[57] as well as Ortega and Espiau.[58]

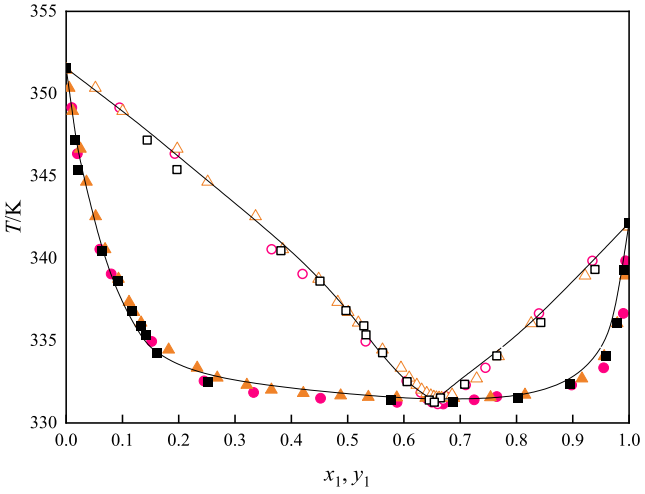

Figure 1. T–x_1–y_1 diagram of *n*-hexane (1) + ethanol (2) at 101.3 kPa: (■) experimental liquid and (□) vapor phase from this work; (pink solid circle) experimental liquid and (pink open circle) vapor phase from the literature;[57] (orange triangle solid) experimental liquid and (orange triangle open) vapor phase from the literature;[58] and (—) regressed with the NRTL model.

Additionally, we measured the pure component vapor pressure for *n*-hexane and ethanol and compared our results with values from the existing literature. The vapor pressure values for *n*-hexane and ethanol obtained from our experiments closely match those reported by Willingham et al.[59] and Kretschmer and Wiebe,[60] as shown in Figures S2 and S3 and tabulated in Table S1 of the Supporting Information. This alignment confirms both the accuracy of our experimental setup and the reliability of the methods. The VLE data was verified for thermodynamic consistency using the method proposed by Van Ness,[51] which confirmed their consistency. A discussion of this consistency test is presented in Section 3.2. Furthermore, the effect of reduced pressure on the relative

Table 3. Constant of the Extended Antoine[a,b]

components	A_1	A_2	A_3	A_4	A_5	$10^6 A_6$	A_7	A_8	A_9
n-hexane	97.742	−6995.5	0	0	−12.702	12.381	2	177.83	507.6
ethanol	66.396	−7122.3	0	0	−7.142	2.885	2	159.05	514.0

[a] Extended Antoine constants: A_1, A_2, A_3, A_4, A_5, A_6, A_7, A_8, and A_9 (physical property databank of Aspen Plus). [b] Extended Antoine: $\ln(P^{\text{sat}}) = A_1 + A_2/(T + A_3) + A_4 T + A_5 \ln T + A_6 T^{A_7}$ for $A_8 < T < A_9$, where P^{sat} is in kPa and T in K.

https://doi.org/10.1021/acs.jced.5c00445
J. Chem. Eng. Data 2025, 70, 4091−4104

volatility of *n*-hexane to ethanol was investigated at pressures of 61.3 and 101.3 kPa. The VLE data for the binary mixture at a reduced pressure of 61.3 kPa were taken from the literature.[58] Figures 2 and S1 indicate that lowering the pressure to 61.3 kPa exerted a negligible effect on the azeotropic behavior of the mixture. The relative volatility is only slightly increased, and the azeotropic point remains in the mixture, shifting just slightly toward the *n*-hexane-rich region. These literature data, combined with the VLE data at 101.3 from this study, were utilized for the regression.

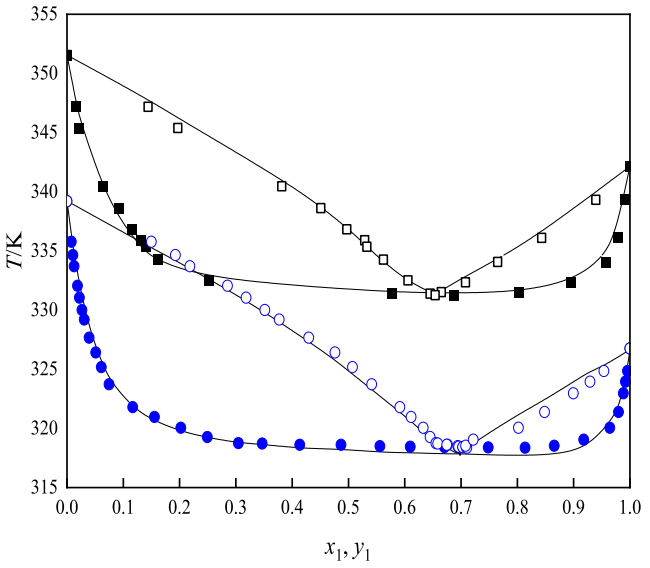

Figure 2. $T-x_1-y_1$ diagram of *n*-hexane (1) + ethanol (2) at pressures of 61.3 and 101.3 kPa: (blue circle solid) experimental liquid and (blue circle open) vapor phase at 61.3 kPa from the literature;[58] (■) experimental liquid and (□) vapor phase at 101.3 kPa from this work; and (—) regressed with the NRTL model.

The setup and methods were then employed to measure the VLE data for the pseudo-ternary mixture of *n*-hexane and ethanol with the entrainers NBP and NMP, respectively. The amount of entrainer added to the mixture on a mass basis is defined by the E/F. The VLE data for the pseudo-ternary mixture of *n*-hexane (1) + ethanol (2) + NBP (3) were measured at E/F = 1, under pressures of 50.0, 80.0, and 100.0 kPa. In addition, measurements were conducted at different E/F values of 2 and 3 at a pressure of 100.0 kPa. The collected VLE data for this pseudo-ternary mixture are presented in Tables 4 and 5, where the liquid phase and the vapor phase mole fraction of *n*-hexane, on an entrainer-free basis, are denoted as x_1' and y_1', respectively. The liquid and vapor phase mole fractions of *n*-hexane, ethanol, and the entrainer are expressed as x_1, x_2, x_3, and y_1, y_2, and y_3, respectively. The equilibrium temperature is represented as T, the activity coefficients of *n*-hexane and ethanol are denoted as γ_1 and γ_2, and the relative volatility of *n*-hexane to ethanol is defined as α_{12}. As no entrainer was detected in the vapor phase, the values of y_3 are considered to be less than 0.0005. Therefore, the values of y_1' are equal to those of y_1.

In addition, the VLE data for the pseudo-ternary mixture of *n*-hexane (1) and ethanol (2), with the benchmark entrainer of NMP, were measured at the E/F = 1 and a pressure of 100.0 kPa. The results of the VLE data are listed in Table 6. The VLE data for both pseudo-ternary mixtures were preferably measured at 100.0 kPa instead of at 101.3 kPa since the laboratory pressure varies within the range of 100.0 and 101.3 kPa. Hence, measurements conducted at 100.0 kPa provide more precise control of the pressure in the setup. The introduction of NBP and NMP into the *n*-hexane and ethanol mixture at all composition ranges studied under the specified E/Fs and pressures resulted in a homogeneous mixture instead of a heterogeneous one, confirming that VLE data measurements can be conducted successfully. For the pseudo-ternary mixture, the activity coefficient of component i (γ_i), which represents nonideal behavior in the liquid phase, was calculated similarly to that of the binary mixture as shown in eq 1. Ideal gas behavior was assumed to occur in these mixtures, since the VLE data were measured at low pressures (atmospheric and vacuum).

Equation 3 was used to calculate the relative volatility of *n*-hexane to ethanol (α_{12}) in the pseudo-ternary mixture of *n*-hexane (1) and ethanol (2) with the presence of NBP and NMP, respectively. The equation employs x_1' and x_2', which represent the liquid phase mole fraction of *n*-hexane and ethanol on an excluded-entrainer basis, as well as y_1 and y_2, which denote the vapor phase mole fraction of *n*-hexane and ethanol.

$$\alpha_{12} = \frac{y_1/x_1'}{y_2/x_2'} \tag{3}$$

The trends observed in the VLE data shown in Table 2, which presents a binary mixture, and Tables 4−6, which depict pseudo-ternary mixtures, provide the following key points: the shifting of the equilibrium temperature, the increasing relative volatility, and the elimination of azeotropes when entrainers are added to the mixtures. These trends are further illustrated in Figures 3−8.

Figure 3 illustrates the effect of reducing the pressure from 100.0 to 80.0 kPa and then to 50.0 kPa on the VLE behavior. The results indicate that decreasing the pressure lowers the equilibrium temperature of the mixture. This occurs because the boiling point of each component in the mixture decreases at lower pressures, resulting in a decrease of the equilibrium temperature within the setup. When E/F = 1 is applied at these pressures, a minimum temperature occurs in the mixture. However, this minimum temperature is not indicative of azeotropic behavior, as the y_1 value does not equal the x_1' value at this temperature. Throughout the three pressures tested, the y_1 values consistently exceed the x_1' values across the entire range of *n*-hexane compositions, confirming the absence of an azeotropic behavior. The minimum temperature phenomenon in this system is driven by strong positive deviations from ideality (primarily due to differences in polarity and hydrogen bonding, which lead to repulsive mixing effects, increasing the activity coefficients), boiling point depression (when the combined vapor pressure of the mixture exceeds that of the pure components due to nonideal mixing), ternary interactions (addition of NBP modifies the binary interactions between *n*-hexane and ethanol), and pressure dependence (at lower pressures the boiling points of all components decrease, but the relative volatility shifts can amplify nonideality, leading to a more pronounced minimum temperature effect). The combination of these phenomena leads to an effective increase in total vapor pressure and thus a lower boiling point at certain compositions, even in the absence of an azeotropic. The phenomena of minimum temperature occurring when the

https://doi.org/10.1021/acs.jced.5c00445
J. Chem. Eng. Data 2025, 70, 4091−4104

Table 4. VLE Data for Hexane (1) + Ethanol (2) + 1-Butylpyrrolidin-2-one (3) with Mass-Based E/F = 1 and Various Pressures at 50.0, 80.0, and 100.0 kPa[a,b,c]

T/K	x_1'	x_1	x_2	x_3	y_1'	y_1	y_2	y_3	γ_1	γ_2	α_{12}
50.0 kPa											
342.20	0.000	0.000	0.754	0.246	0.000	0.000	1.000	0.000		0.954	
333.50	0.096	0.071	0.668	0.261	0.399	0.399	0.601	0.000	3.633	0.941	6.26
332.04	0.114	0.084	0.652	0.264	0.451	0.451	0.549	0.000	3.659	0.941	6.42
325.59	0.231	0.166	0.552	0.282	0.681	0.681	0.319	0.000	3.465	0.869	7.10
323.71	0.287	0.224	0.486	0.290	0.730	0.730	0.270	0.000	2.942	0.914	6.70
321.64	0.474	0.310	0.374	0.316	0.805	0.805	0.195	0.000	2.526	0.946	4.58
321.72	0.621	0.413	0.252	0.335	0.867	0.867	0.133	0.000	2.035	0.956	3.98
322.05	0.691	0.450	0.207	0.343	0.881	0.881	0.119	0.000	1.878	1.021	3.31
323.14	0.799	0.516	0.127	0.357	0.928	0.928	0.072	0.000	1.656	0.961	3.24
323.90	0.908	0.569	0.062	0.369	0.964	0.964	0.036	0.000	1.520	0.955	2.68
325.29	1.000	0.621	0.000	0.379	1.000	1.000	0.000	0.000	1.376		
80.0 kPa											
353.50	0.000	0.000	0.754	0.246	0.000	0.000	1.000	0.000		0.967	
346.58	0.094	0.070	0.669	0.261	0.408	0.408	0.592	0.000	3.999	0.849	6.62
346.01	0.107	0.079	0.658	0.263	0.413	0.413	0.587	0.000	3.648	0.876	5.89
341.35	0.204	0.148	0.575	0.277	0.613	0.613	0.387	0.000	3.334	0.802	6.17
339.96	0.242	0.174	0.543	0.283	0.654	0.654	0.346	0.000	3.150	0.807	5.91
335.70	0.467	0.320	0.365	0.315	0.768	0.768	0.232	0.000	2.305	0.966	3.77
334.99	0.643	0.427	0.236	0.337	0.843	0.843	0.157	0.000	1.943	1.042	2.99
335.34	0.683	0.449	0.209	0.342	0.857	0.857	0.143	0.000	1.855	1.059	2.78
336.67	0.788	0.509	0.136	0.355	0.908	0.908	0.092	0.000	1.661	0.991	2.64
337.94	0.903	0.572	0.060	0.368	0.957	0.957	0.043	0.000	1.497	0.993	2.39
339.58	1.000	0.621	0.000	0.379	1.000	1.000	0.000	0.000	1.367		
100.0 kPa											
359.46	0.000	0.000	0.754	0.246	0.000	0.000	1.000	0.000		0.963	
350.71	0.090	0.067	0.673	0.260	0.365	0.365	0.635	0.000	4.116	0.959	5.83
349.81	0.112	0.082	0.654	0.264	0.396	0.396	0.604	0.000	3.732	0.973	5.21
345.10	0.203	0.146	0.577	0.277	0.586	0.586	0.414	0.000	3.590	0.914	5.58
342.45	0.366	0.255	0.445	0.301	0.709	0.709	0.291	0.000	2.699	0.930	4.24
341.86	0.443	0.305	0.384	0.311	0.748	0.748	0.252	0.000	2.421	0.959	3.73
342.24	0.645	0.427	0.235	0.338	0.833	0.833	0.167	0.000	1.904	1.017	2.75
342.56	0.691	0.447	0.210	0.343	0.842	0.842	0.158	0.000	1.821	1.065	2.39
343.77	0.795	0.513	0.131	0.356	0.900	0.900	0.100	0.000	1.634	1.033	2.31
345.05	0.904	0.571	0.061	0.368	0.954	0.954	0.046	0.000	1.495	0.974	2.20
347.02	1.000	0.621	0.000	0.379	1.000	1.000	0.000	0.000	1.358		

[a] T: equilibrium temperature; x_1': mole fraction of *n*-hexane in the liquid phase (NBP-free basis); y_1': mole fraction of *n*-hexane in the vapor phase (NBP-free basis); x_1, x_2, and x_3: mole fractions of *n*-hexane, ethanol, and NBP in the liquid phase, respectively; y_1, y_2, and y_3: mole fractions of *n*-hexane, ethanol, and NBP in the vapor phase; γ_1 and γ_2: activity coefficient of *n*-hexane and ethanol, respectively: α_{12}: relative volatility of *n*-hexane to ethanol. [b] Expanded combined uncertainties (U with $k = 2$): $U(T) = 0.40$ K, $U(P) = 0.23$ kPa, and $U(x_1) = U(y_1) = 0.006$. [c] y_3 values are less than 0.0005.

azeotropic point is absent have also been reported in studies involving mixtures of water and acetonitrile with the addition of entrainers such as ethylene glycol[61] and dimethyl sulfoxide,[62] mixtures of methyl propionate and ethanol with ionic liquids,[63] as well as in the mixture of 2-butanone and ethanol in the presence of ionic liquids.[64,65]

The effect of the amount of entrainer in the mixture on the equilibrium temperature was investigated. As illustrated in Figure 4, when the mass of the NBP is increased from E/F = 1 to 2 and 3 at a constant pressure of 100.0 kPa, the equilibrium temperature also increases compared to that without the entrainer. The addition of a larger mass of NBP to the mixture causes the entrainer to dominate the liquid composition. Furthermore, NBP has a stronger interaction with ethanol. The stronger interaction is mainly due to hydrogen bonding between the hydroxyl group of ethanol, which acts as a hydrogen bond donor, and the carbonyl group of the pyrrolidone ring in NBP, which serves as a hydrogen bond acceptor. In contrast, the interaction with *n*-hexane is governed by weaker van der Waals forces due to the nonpolar nature of *n*-hexane. These two causes lead to a decrease in the vaporization of both *n*-hexane and ethanol. As a result, an elevated temperature is needed to evaporate *n*-hexane and ethanol in order to achieve the equilibrium conditions, resulting in an increase in the equilibrium temperature of the mixture. Figure 4 also indicates that the minimum temperature occurs at E/Fs = 1 and 2, even though the azeotropic point is already removed, as demonstrated in Figure 6. However, the minimum temperature nearly disappears at E/F = 3.

The effect of the presence of NBP on breaking the azeotropic behavior in a mixture of *n*-hexane and ethanol is demonstrated in the $x_1'-y_1$ diagrams shown in Figures 5 and 6. The addition of NBP to this mixture alters its nonideal behavior by modifying the molecular interactions between the

https://doi.org/10.1021/acs.jced.5c00445
J. Chem. Eng. Data 2025, 70, 4091−4104

Table 5. VLE Data for Hexane (1) + Ethanol (2) + 1-Butylpyrrolidin-2-one (3) at Pressure of 100.0 kPa with Mass-Based E/F = 2 and 3[a,b,c]

T/K	x_1'	x_1	x_2	x_3	y_1'	y_1	y_2	y_3	γ_1	γ_2	α_{12}
					E/F = 2						
369.53	0.000	0.000	0.605	0.395	0.000	0.000	1.000	0.000		0.834	
361.33	0.082	0.048	0.540	0.412	0.275	0.275	0.725	0.000	3.201	0.910	4.22
353.98	0.157	0.090	0.484	0.426	0.539	0.539	0.461	0.000	4.112	0.851	6.31
351.20	0.224	0.126	0.436	0.438	0.624	0.624	0.376	0.000	3.692	0.859	5.75
349.31	0.355	0.191	0.348	0.461	0.734	0.734	0.266	0.000	3.025	0.824	5.01
348.97	0.477	0.248	0.272	0.480	0.801	0.801	0.199	0.000	2.570	0.796	4.42
349.14	0.659	0.326	0.167	0.507	0.878	0.878	0.122	0.000	2.133	0.791	3.71
349.41	0.808	0.399	0.074	0.527	0.947	0.947	0.053	0.000	1.863	0.771	4.20
350.10	0.913	0.423	0.037	0.540	0.972	0.972	0.028	0.000	1.768	0.797	3.26
350.93	1.000	0.450	0.000	0.550	1.000	1.000	0.000	0.000	1.668		
					E/F = 3						
380.85	0.000	0.000	0.505	0.495	0.000	0.000	1.000	0.000		0.682	
375.24	0.091	0.044	0.442	0.514	0.257	0.257	0.743	0.000	2.252	0.698	3.45
372.51	0.142	0.068	0.408	0.524	0.459	0.459	0.541	0.000	2.819	0.603	5.12
369.28	0.224	0.123	0.338	0.539	0.616	0.616	0.384	0.000	2.266	0.579	5.57
367.74	0.289	0.133	0.316	0.551	0.648	0.648	0.352	0.000	2.296	0.598	4.52
365.12	0.413	0.177	0.252	0.571	0.742	0.742	0.258	0.000	2.116	0.604	4.10
363.01	0.625	0.249	0.149	0.602	0.869	0.869	0.131	0.000	1.866	0.560	3.97
362.28	0.705	0.274	0.114	0.612	0.903	0.903	0.097	0.000	1.796	0.557	3.90
361.95	0.803	0.302	0.074	0.624	0.941	0.941	0.059	0.000	1.717	0.524	3.95
362.00	0.913	0.331	0.032	0.637	0.975	0.975	0.025	0.000	1.616	0.524	3.66
362.19	1.000	0.353	0.000	0.647	1.000	1.000	0.000	0.000	1.547		

[a]T: equilibrium temperature; x_1': mole fraction of *n*-hexane in the liquid phase (NBP-free basis); y_1': mole fraction of *n*-hexane in the vapor phase (NBP-free basis); x_1, x_2, and x_3: mole fractions of *n*-hexane, ethanol, and NBP in the liquid phase, respectively; y_1, y_2, and y_3: mole fractions of *n*-hexane, ethanol, and NBP in the vapor phase; γ_1 and γ_2: activity coefficient of *n*-hexane and ethanol, respectively: α_{12}: relative volatility of *n*-hexane to ethanol. [b]Expanded combined uncertainties (U with $k = 2$): $U(T) = 0.40$ K, $U(P) = 0.23$ kPa, and $U(x_1) = U(y_1) = 0.006$. [c]y_3 values are less than 0.0005.

Table 6. VLE Data for *n*-Hexane (1) + Ethanol (2) + 1-Methylpyrrolidin-2-one (3) with Mass-Based E/F = 1 and Pressure at 100.0 kPa[a,b,c]

T/K	x_1'	x_1	x_2	x_3	y_1'	y_1	y_2	y_3	γ_1	γ_2	α_{12}
362.49	0.000	0.000	0.683	0.317	0.000	0.000	1.000	0.000		0.951	
354.18	0.067	0.044	0.626	0.330	0.255	0.255	0.745	0.000	3.926	1.056	4.77
350.65	0.096	0.064	0.601	0.335	0.438	0.438	0.562	0.000	5.181	0.952	7.33
344.98	0.145	0.095	0.561	0.344	0.601	0.601	0.399	0.000	5.676	0.909	8.92
344.01	0.159	0.104	0.550	0.346	0.637	0.637	0.363	0.000	5.667	0.880	9.30
341.71	0.240	0.154	0.486	0.360	0.724	0.724	0.276	0.000	4.674	0.833	8.32
340.12	0.350	0.218	0.404	0.378	0.781	0.781	0.219	0.000	3.735	0.850	6.63
339.99	0.465	0.282	0.323	0.395	0.819	0.819	0.181	0.000	3.044	0.884	5.21
340.29	0.610	0.358	0.226	0.416	0.882	0.882	0.118	0.000	2.556	0.816	4.78
340.82	0.683	0.393	0.181	0.426	0.899	0.899	0.101	0.000	2.337	0.846	4.15
341.87	0.780	0.441	0.120	0.439	0.931	0.931	0.069	0.000	2.087	0.833	3.82
343.29	0.886	0.488	0.060	0.452	0.964	0.964	0.036	0.000	1.867	0.827	3.41
344.12	0.956	0.518	0.022	0.460	0.983	0.983	0.017	0.000	1.749	0.987	2.73
344.77	1.000	0.535	0.000	0.465	1.000	1.000	0.000	0.000	1.688		

[a]T: equilibrium temperature; x_1': mole fraction of *n*-hexane in the liquid phase (NMP-free basis); y_1': mole fraction of *n*-hexane in the vapor phase (NMP-free basis); x_1, x_2, and x_3: mole fractions of *n*-hexane, ethanol, and NMP in the liquid phase, respectively; y_1, y_2, and y_3: mole fractions of *n*-hexane, ethanol, and NMP in the vapor phase; γ_1 and γ_2: activity coefficient of *n*-hexane and ethanol, respectively: α_{12}: relative volatility of *n*-hexane to ethanol. [b]Expanded combined uncertainties (U with $k = 2$): $U(T) = 0.40$ K, $U(P) = 0.23$ kPa, and $U(x_1) = U(y_1) = 0.006$. [c]y_3 values are less than 0.0005.

components. Ethanol is a polar component, while *n*-hexane is nonpolar. Due to its polar nature, NBP interacts more favorably with ethanol than with *n*-hexane. This preferential interaction effectively reduces the interaction between *n*-hexane and ethanol, leading to an increase in the relative volatility and eliminating the azeotropic behavior. As a result, *n*-hexane can be separated more efficiently from ethanol. Tables 4 and 5 show that the introduction of NBP results in a lower activity coefficient for ethanol (γ_2) compared to that for *n*-hexane (γ_1). This signifies that NBP interacts more strongly with ethanol than with *n*-hexane. Consequently, the volatility of *n*-hexane increases, allowing it to be more easily separated from ethanol.

https://doi.org/10.1021/acs.jced.5c00445
J. Chem. Eng. Data 2025, 70, 4091−4104

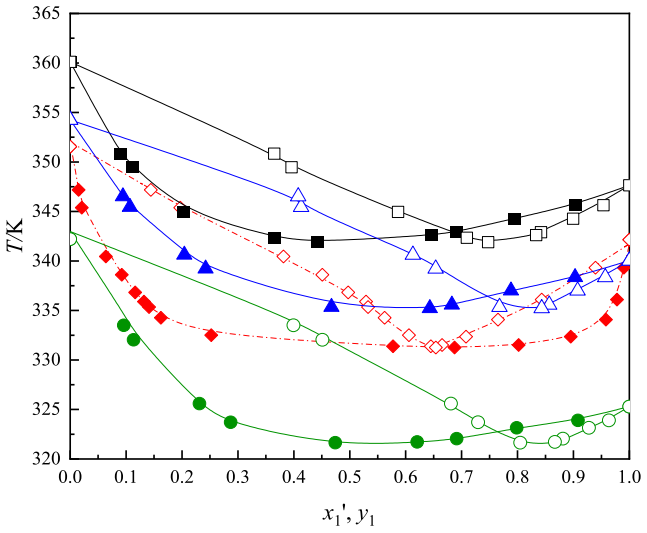

Figure 3. $T-x_1'-y_1$ diagram of *n*-hexane (1) + ethanol (2) + 1-butylpyrrolidin-2-one (3) for the experimental data with E/F = 1: (■) x_1' and (□) y_1 at 100.0 kPa; (blue triangle solid) x_1' and (blue open triangle) y_1 at 80.0 kPa; (green solid circle) x_1' and (green open circle) y_1 at 50.0 kPa; and (red diamond solid) x_1 and (red diamond open) y_1 for the binary mixture at 101.3 kPa. Regressed with the NRTL model: (—) 100.0 kPa (black); 80.0 kPa (blue); 50.0 kPa (green); and (black solid); (---) binary mixture at 101.3 kPa (red).

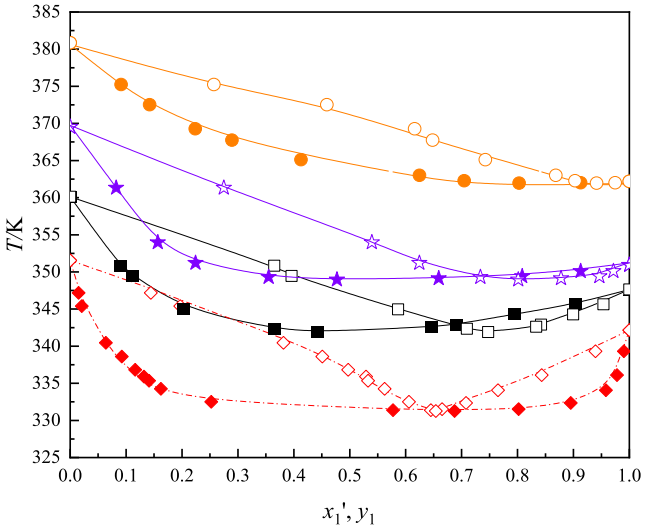

Figure 4. $T-x_1'-y_1$ diagram of *n*-hexane (1) + ethanol (2) + 1-butylpyrrolidin-2-one (3) for the experimental data at pressure of 100.0 kPa: (■) x_1' and (□) y_1 for E/F = 1; (purple star solid) x_1' and (purple star open) y_1 for E/F = 2; (orange circle solid) x_1' and (orange circle open) y_1 for E/F = 3; and (red diamond solid) x_1 and (red diamond open) y_1 for the binary mixture (E/F = 0) at 101.3 kPa. Regressed with the NRTL model: (—) E/F = 1 (black); E/F = 2 (purple); E/F = 3 (orange); and (---) binary mixture at 101.3 kPa (red).

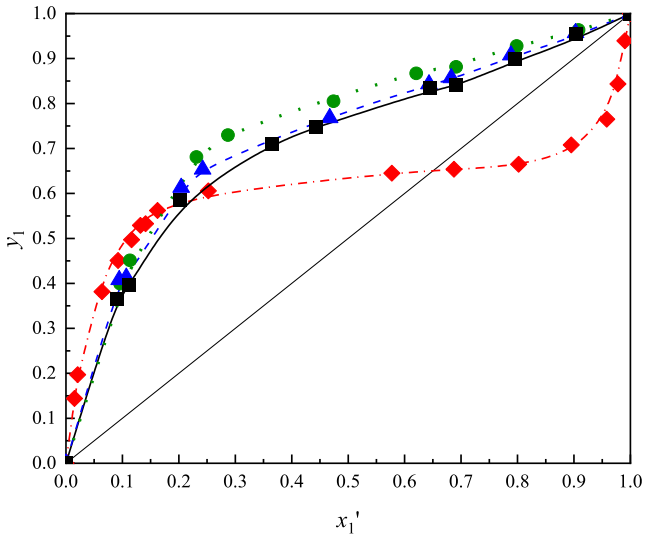

Figure 5. $x_1'-y_1$ diagram of *n*-hexane (1) + ethanol (2) + 1-butylpyrrolidin-2-one (3) for the experimental data with E/F = 1: (■) at 100.0 kPa; (blue triangle solid) at 80.0 kPa; (green solid circle) at 50.0 kPa; and (red diamond solid) binary mixture at 101.3 kPa. Regressed with the NRTL model: (—) 100.0 kPa; (blue dashed line) 80.0 kPa; (green dotted line) 50.0 kPa; and (red dash-dotted line) binary mixture at 101.3 kPa.

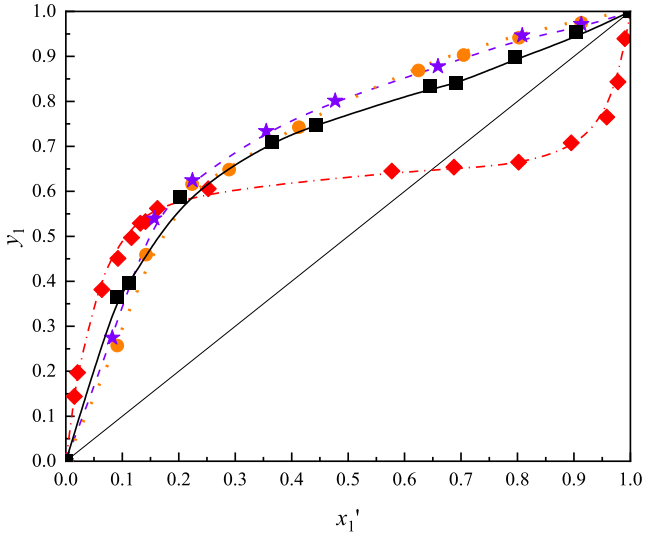

Figure 6. $x_1'-y_1$ diagram of *n*-hexane (1) + ethanol (2) + 1-butylpyrrolidin-2-one (3) for the experimental data at pressure of 100.0 kPa: (■) E/F = 1; (purple star solid) E/F = 2; (orange circle solid) E/F = 3; and (red diamond solid) binary mixture at 101.3 kPa. Regressed with the NRTL model: (—) E/F = 1; (purple dashed line) E/F = 2; (orange dotted line) E/F = 3; and (red dash-dotted line) binary mixture at 101.3 kPa.

In this study, the effect of pressure on relative volatility was investigated. As shown in Figure 5, the addition of NBP with an E/F = 1 at various pressures of 100.0, 80.0, and 50.0 kPa, respectively, was found to increase the relative volatility of *n*-hexane to ethanol, effectively removing the azeotropic point. As the pressure decreases from 100.0 to 80.0 and 50.0 kPa, the relative volatility of *n*-hexane to ethanol increases. Lower pressure results in a lower equilibrium temperature, which elevates the nonideality of the mixture and contributes to the increased relative volatility. However, when pressure is reduced to 80.0 and 50.0 kPa, the increase in the relative volatility levels off, as the interaction between NBP and ethanol tends not to considerably increase at these lower pressures. This is confirmed in Table 4, which shows that the activity coefficient of ethanol (γ_2) slightly decreases when the pressure is lowered from 100.0 to 80.0 and 50.0 kPa.

This work also examined the effect of the NBP concentration on the relative volatility. Similar to the influence

https://doi.org/10.1021/acs.jced.5c00445
J. Chem. Eng. Data 2025, 70, 4091−4104

of pressure, Figure 6 shows that increasing the E/F from 1 to 2 and 3 results only in a modest increase of the relative volatility. Furthermore, the relative volatility remained unchanged when the E/F ratio was increased from 2 to 3. As detailed in Table 5, increasing the amount of NBP enhances the interaction between NBP and ethanol, which is confirmed by the decrease in the activity coefficient of ethanol (γ_2). However, the nonideality of *n*-hexane decreases with an increase in the amount of NBP as the activity coefficient of *n*-hexane (γ_1) decreases. This corresponds to the significant rise in the equilibrium temperature. The combination of both effects contributes to the overall slight increase in relative volatility.

NMP as a benchmark entrainer was also evaluated in this work. It was added to an azeotropic mixture of *n*-hexane and ethanol with an E/F of 1 and a pressure of 100.0 kPa. As depicted in Figure 7, the introduction of NMP leads to an

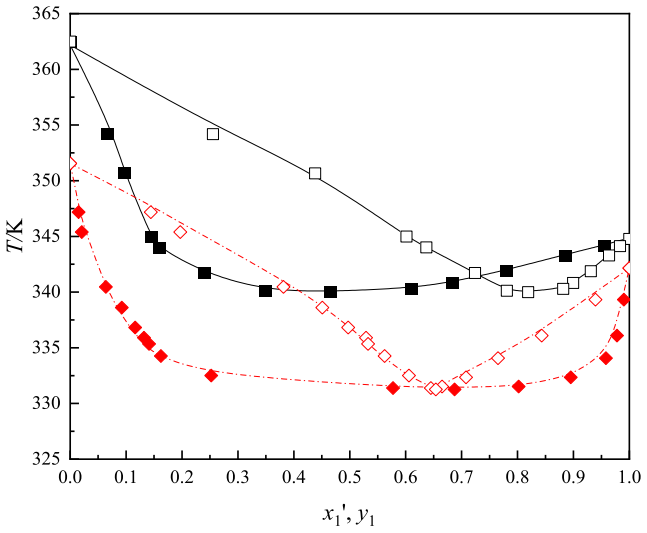

Figure 7. $T-x_1'-y_1$ diagram of *n*-hexane (1) + ethanol (2) + 1-methylpyrrolidin-2-one (3) for the experimental data with E/F = 1: (■) x_1' and (□) y_1 at 100.0 kPa; and (red diamond solid) x_1 and (red diamond open) y_1 for the binary mixture at 101.3 kPa. Regressed with the NRTL model: (—) 100.0 kPa (black); and (···) binary mixture at 101.3 kPa (red).

elevated equilibrium temperature when compared to binary mixture without entrainer, a trend similar to that observed with the addition of NBP. NMP has a higher boiling point than both *n*-hexane and ethanol, and it becomes the dominant component in the liquid phase when NMP is added with an E/F = 1. Additionally, NMP exhibits a stronger interaction with ethanol. These situations result in reduced vaporization of the mixture, thus requiring a higher temperature to reach equilibrium.

As shown in Figure 8, the presence of NMP in the mixture effectively elevates the relative volatility and eliminates the azeotropic point. Similar to NBP, as a polar entrainer, NMP is more likely to interact with a polar component than a nonpolar one. Hence, NMP has a stronger interaction with ethanol compared to that with *n*-hexane. This is indicated in Table 6, where the activity coefficient of ethanol (γ_2) is lower than that of *n*-hexane (γ_1). The stronger interaction between NMP and ethanol weakens the original interaction between *n*-hexane and ethanol, resulting in easier vaporization of *n*-hexane. This promotes a more effective separation of *n*-hexane from toluene. In our previous work, we examined molecular interactions

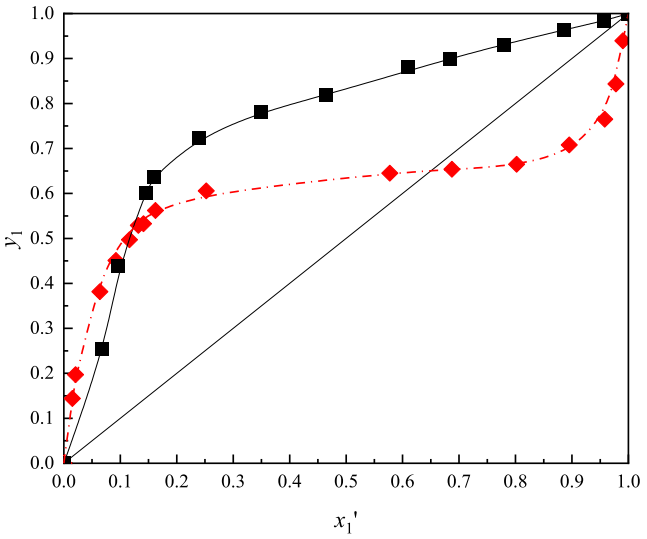

Figure 8. $x_1'-y_1$ diagram of *n*-hexane (1) + ethanol (2) + 1-methylpyrrolidin-2-one (3) for the experimental data: (■) E/F = 1 at 100.0 kPa and (red diamond solid) binary mixture at 101.3 kPa. Regressed with the NRTL model: (—) E/F = 1 at 100.0 kPa; and (red dash-dotted line) binary mixture at 101.3 kPa.

using unimolecular quantum chemical calculations (COSMO-RS) to better understand the polar roles of the NBP and NMP. The results indicated that both NBP and NMP, as polar compounds, exhibited stronger interaction with the compounds that have more polar behavior.[15] Additionally, we compared the binary end points of the VLE data for *n*-hexane–NMP from our study with existing literature, as illustrated in Figure S4 of the Supporting Information. The data from our work demonstrates good agreement with the literature data,[66,67] confirming the reliability of our results.

These VLE results are fundamental for the design of extractive distillation processes. However, their direct application to a real extractive distillation column has inherent limitations. This is because the VLE data do not consider the mass transfer resistance that occurs at the vapor–liquid interfaces in the actual column. Moreover, while the entrainer concentration in the VLE is assumed to be uniform, in a real extractive distillation column, the entrainer concentration varies stage by stage. Therefore, while promising, the translation of these VLE data to full-scale operations requires further validation through rigorous process simulation or pilot-scale experiments.

To compare the performance of NBP and NMP in increasing relative volatility, we analyzed the relative volatility of NBP under various E/Fs and pressures with NMP at E/F = 1 and a pressure of 100.0 kPa, specifically at the azeotropic point, where the mole fraction of *n*-hexane on an entrainer-free basis is x_1' = 0.66. In the binary mixture, the relative volatility at the azeotropic point is 1, meaning that the mole fraction *n*-hexane in the liquid phase is equal to that in the vapor phase. Figure 9 shows that the NBP with an E/F of 1 and a pressure of 50.0 kPa, as well as NBP with E/Fs of 2 and 3 at a pressure of 100.0 kPa, exhibit comparable relative volatility to NMP with an E/F of 1 at a pressure of 100.0 kPa.

At E/F = 1 and a pressure of 100.0 kPa, NMP demonstrates a higher relative volatility compared to NBP. This indicates a stronger interaction between NMP and ethanol, as the activity coefficient of ethanol (γ_2) is lower, as shown in Table 6,

https://doi.org/10.1021/acs.jced.5c00445
J. Chem. Eng. Data 2025, 70, 4091−4104

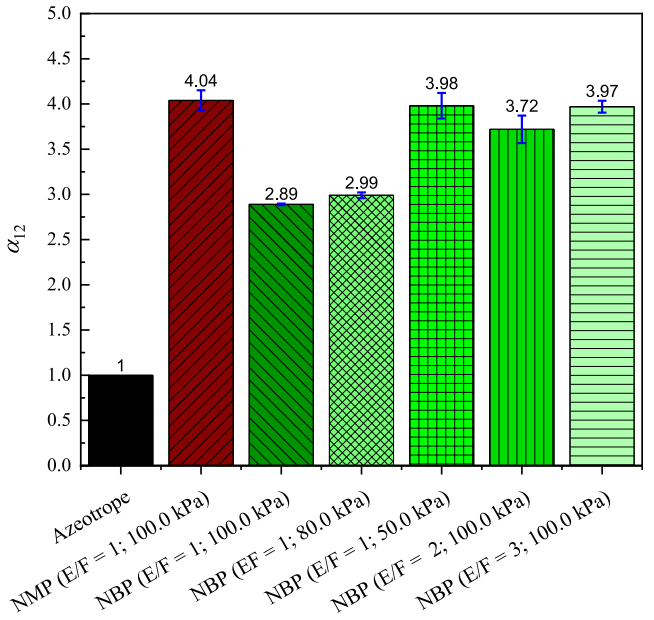

Figure 9. Relative volatility of *n*-hexane (1) to ethanol (2) (α_{12}) containing entrainer of NMP at E/F = 1 and a pressure of 100.0 kPa and NBP at various E/Fs and pressures. The relative volatility was measured at an azeotropic point (mole fraction of *n*-hexane on an entrainer-free basis; $x_1' = 0.66$).

compared to that in NBP in Table 4. This facilitates easier separation of *n*-hexane. When NBP is applied at E/F = 1 and at a reduced pressure of 50.0 kPa or at higher E/Fs of 2 and 3 at 100.0 kPa, its relative volatility becomes comparable, which is slightly lower than that of NMP. The lower pressure decreases equilibrium temperature, enhances the interaction between NBP and ethanol, and increases the nonideality of the mixture, both of which favor the separation of *n*-hexane from ethanol. Similarly, increasing the E/F strength strengthens the interaction between NBP and ethanol, as shown in Table 5, further increasing relative volatility. A slightly lower relative volatility can result in a higher number of stages and reflux ratio required in an extractive distillation column, contributing to increased energy consumption. However, operating at lower pressures can reduce the reboiler temperature, which in turn decreases the energy requirements.

Furthermore, NBP has a boiling point higher than that of NMP, which provides higher thermal stability and can minimize entrainer loss in extractive distillation. Environmentally, NBP is categorized as nontoxic, biodegradable, and free from reproductive toxicity. These relative volatility, thermal, and environmental benefits highlight the promising performance of NBP, as a greener entrainer, presenting a viable alternative to NMP, as a conventional entrainer, for separating *n*-hexane from ethanol via extractive distillation. This suggests that the utilization of NBP as a greener entrainer could contribute to the development of more sustainable and green extractive distillation processes.

3.2. Thermodynamic Consistency Tests. The consistency of the investigated VLE data was evaluated using the Van Ness thermodynamic consistency test.[51]

$$\Delta P = \frac{1}{n_p} \times \sum_{i=1}^{n_p} \Delta P_i = \frac{1}{n_p} \times \sum_{i=1}^{n_p} 100 \times \left| \frac{P_i^{cal} - P_i^{exp}}{P_i^{exp}} \right| \quad (4)$$

$$\Delta y = \frac{1}{n_p} \times \sum_{i=1}^{n_p} \Delta y_i = \frac{1}{n_p} \times \sum_{i=1}^{n_p} 100 \times |y_i^{cal} - y_i^{exp}| \quad (5)$$

This test ensured the reliability of the VLE data. The Van Ness method is mathematically represented in eqs 4 and 5, where the pressure, the number of data, and mole fraction in vapor phase are denoted as P, n_p, and y, respectively. Moreover, the values calculated from the NRTL model and those obtained from the experimental work are represented as cal and exp, respectively. According to the Van Ness method, a data set is classified as consistent if both ΔP and Δy values are less than 1. As presented in Table 7, the values for ΔP and Δy for the studied binary mixture and the pseudo-ternary mixtures fall below this threshold. The detailed values of ΔP and Δy for the investigated mixtures are provided in Tables S2−S4 in the Supporting Information. Furthermore, the $\ln(\gamma_1/\gamma_2)$ residual distribution must demonstrate random behavior to satisfy Van Ness criteria. As shown in Figures S5−S7 in the Supporting Information, the results of the $\ln(\gamma_1/\gamma_2)$ residual distribution verify this randomness. These findings affirm the thermodynamic consistency of the VLE data obtained in this study.

Table 7. Thermodynamic Consistency Test Results

mixture	Δy^a	ΔP^b	results
n-hexane (1) + ethanol (2)	0.6	0.4	passed
n-hexane (1) + ethanol (2) + NBP (3)	0.5	0.8	passed
n-hexane (1) + ethanol (2) + NMP (3)	0.4	0.8	passed

a $\Delta y = \frac{1}{n_p} \times \sum_{i=1}^{n_p} \Delta y_i = \frac{1}{n_p} \times \sum_{i=1}^{n_p} 100 \times |y_i^{cal} - y_i^{exp}| < 1$

b $\Delta P = \frac{1}{n_p} \times \sum_{i=1}^{n_p} \Delta P_i = \frac{1}{n_p} \times \sum_{i=1}^{n_p} 100 \times \left| \frac{P_i^{cal} - P_i^{exp}}{P_i^{exp}} \right| < 1$

3.3. VLE Data Correlation. The investigated VLE data was regressed to obtain the optimum BIPs. In this regression, NRTL, as a widely adopted thermodynamic model, was employed. This model is well-regarded for its ability to accurately represent the mixture involving entrainers, often yielding excellent agreement with experimental results.[33,68−73] Furthermore, our previous study demonstrated that the NRTL model exhibits more accurate correlation results than the UNIQUAC model.[27] The NRTL model is expressed in eq 6.

$$\ln \gamma_i = \frac{\sum_{j=1}^{n_c} x_j \tau_{ji} G_{ji}}{\sum_{k=1}^{n_c} x_k G_{ki}} + \sum_{j=1}^{n_c} \frac{x_j G_{ij}}{\sum_{k=1}^{N} x_k G_{kj}} \left(\tau_{ij} - \frac{\sum_{m=1}^{n_c} x_m \tau_{mj} G_{mj}}{\sum_{k=1}^{n_c} x_k G_{kj}} \right) \quad (6)$$

where the activity coefficient for component i is expressed as γ_i and the total number of components is denoted as n_c. In this model, the parameters are explained as outlined in eq 7, where C_{ij} indicates the constant of nonrandomness in the binary interaction for the component $i-j$.

$$G_{ij} = \exp(-C_{ij}\tau_{ij}); \quad \tau_{ij} = A_{ij} + B_{ij}/T; \quad G_{ii} = 1; \quad \tau_{ii} = 0 \quad (7)$$

https://doi.org/10.1021/acs.jced.5c00445
J. Chem. Eng. Data 2025, 70, 4091−4104

Table 8. NRTL Binary Interaction Parameters for Hexane (1) + Ethanol (2) + 1-Butylpyrrolidin-2-one (3) and Hexane (1) + Ethanol (2) + 1-Methylpyrrolidin-2-one (3)[a,b]

i component	j component	A_{ij}	A_{ji}	B_{ij}/K	B_{ji}/K	C_{ij}
n-hexane (1)[c]	ethanol (2)	−10.342	−3.854	4120.934	1829.392	0.47
n-hexane (1)	1-butylpyrrolidin-2-one (3)	1.748	−13.206	−581.379	5130.115	0.05
ethanol (2)	1-butylpyrrolidin-2-one (3)	22.377	−1.069	−5518.982	−133.055	0.45
n-hexane (1)	1-methylpyrrolidin-2-one (3)	−20.689	413.501	7863.726	9869.500	0.03
ethanol (2)	1-methylpyrrolidin-2-one (3)	19.225	5.003	−5179.301	−2561.179	0.30

[a] A_{ij}, A_{ji}, B_{ij}, and B_{ji}: asymmetric parameters; C_{ij}: constant of nonrandomness. [b] NRTL model: $\tau_{ij} = A_{ij} + B_{ij}/T$. [c] The BIPs for the hexane (1)−ethanol (2) pair were derived from the correlation of the VLE data at 101.3 kPa from this work combined with the VLE data at 61.3 kPa from the literature.[58]

Table 9. Root-Mean-Square Deviation (RMSD)[a]

	RMSD[b]			
	T/K	P/kPa	x_1'	y_1
n-hexane (1) + ethanol (2)	0.38	0.5	0.003	0.007
n-hexane (1) + ethanol (2) + 1-butylpyrrolidin-2-one (3)	0.32	0.6	0.003	0.007
n-hexane (1) + ethanol (2) + 1-methylpyrrolidin-2-one (3)	0.12	0.9	0.003	0.009

[a] T: temperature, P: pressure; x_1': mole fraction of *n*-hexane in the liquid phase (entrainer-free basis), y_1: mole fraction of *n*-hexane in the vapor phase. [b] RMSD: $\Delta M = \sqrt{\frac{1}{n}\sum_{i=1}^{n}(M_{exp} - M_{cal})^2}$, where n denotes the number of data points; M corresponds to T, P, x_1', and y_1, respectively.

The BIPs for the *n*-hexane and ethanol pair were obtained by regressing the VLE data of the binary mixture of *n*-hexane and ethanol at pressures of 61.3 and 101.3 kPa. The VLE data at 61.3 kPa was retrieved from the literature,[58] while the data at 101.3 kPa was obtained from this work. These VLE data sets were simultaneously regressed to determine the optimum BIPs for the *n*-hexane and ethanol pair. The resulting BIPs were then applied to regress the VLE data of the pseudo-ternary mixture of *n*-hexane and ethanol containing NBP and NMP, respectively. As the experimental VLE data for *n*-hexane and ethanol with the presence of NBP were collected over a pressure range of 50.0−100.0 kPa, the regression of the binary mixture was conducted using data from both atmospheric and reduced pressure to ensure that the BIPs for *n*-hexane and ethanol pair accurately captured the temperature range relevant to this pseudo-ternary mixture. For the binary mixture of *n*-hexane−ethanol regression, the nonrandomness parameter of the NRTL model (C_{ij}) was fixed at a value of 0.47. In contrast, for the pseudo-ternary mixture regression, C_{ij} was treated as an adjustable parameter rather than being fixed. This approach provides greater flexibility, leading to an improved regression accuracy. Initially, we attempted to correlate the pseudo-ternary mixture data using a fixed value of 0.3. Unfortunately, this approach did not yield satisfactory results due to the strong nonideal behavior of the system, which caused the value to deviate from 0.3. We then evaluated a fixed value of 0.2, but this also resulted in inaccurate correlation since it only represented the *n*-hexane-entrainer pair and not the ethanol−entrainer pair. Moreover, we assessed a fixed value of 0.47; however, this value did not adequately represent the *n*-hexane−entrainer or ethanol−entrainer pairs, as it was primarily applicable to the pair of nonpolar, strongly self-associated substances. Therefore, the correlation results were not in good agreement with the experimental data when using fixed values. As a result, we opted to regress this parameter for both *n*-hexane−entrainer and ethanol−entrainer pairs to obtain a more accurate correlation. In addition, the A_{ij} and A_{ji} parameters were involved as adjustable variables in the regression, as this enhanced the correlation results. In the regression, the optimization of BIPs was obtained by minimizing the objective function (OF) using the maximum likelihood-based algorithm developed by Britt and Luecke.[74] The formulation of the objective function is presented in eq 8.

$$\mathrm{OF} = \sum_{k=1}^{n_p} \left\{ \left| \frac{P_k^{cal} - P_k^{exp}}{\sigma_P} \right|^2 + \left| \frac{T_k^{cal} - T_k^{exp}}{\sigma_T} \right|^2 + \left| \frac{x_{1,k}^{cal} - x_{1,k}^{exp}}{\sigma_x} \right|^2 + \left| \frac{y_{1,k}^{cal} - y_{1,k}^{exp}}{\sigma_y} \right|^2 \right\} \quad (8)$$

Here, the total number of data points is defined by n_p and the standard deviation is represented by σ. The optimum BIPs for all component pairs obtained from the regression are summarized in Table 8.

The regression result from the NRTL model accurately represents the experimental data for both the binary mixture of *n*-hexane and ethanol and the pseudo-ternary mixtures of *n*-hexane and ethanol with the addition of NBP and NMP, respectively. For the pseudo-ternary mixture containing NBP, the VLE data at all E/Fs and pressures were regressed together to obtain the BIPs, which accurately describe the system over a wide range of entrainer compositions and various pressures. Figure 2 shows the regression results for the binary mixture, while Figures 3 and 4 illustrate the results for the pseudo-ternary mixture with the presence of NBP, and Figure 7 demonstrates the results for the mixture containing NMP. The good agreements observed are further confirmed by the low values of the root-mean-square deviations for each mixture, as listed in Table 9. The residual plots of liquid and vapor mole fraction and temperature are listed in Figures S8−S16 in the Supporting Information file. These results confirm that the NRTL model, along with the optimum BIPs, can be reliably applied for the process simulation of extractive distillation to separate the azeotropic mixture of *n*-hexane and ethanol using the greener entrainer NBP as well as the benchmark entrainer NMP.

https://doi.org/10.1021/acs.jced.5c00445
J. Chem. Eng. Data 2025, 70, 4091−4104

4. CONCLUSIONS

In conclusion, the VLE data for the binary *n*-hexane−ethanol mixture as well as, for the first time, pseudomixtures of *n*-hexane−ethanol containing NBP and NMP as entrainers were measured in this study. The experimental setup and procedure were validated, confirming that they are suitable for measuring the VLE data of the investigated mixtures. The VLE data for both binary and pseudomixtures were found to be consistent as they passed the thermodynamic consistency test. This suggests that the VLE data provided in this work are reliable.

Furthermore, the results demonstrated that the presence of NBP and NMP can increase the relative volatility and remove the azeotropic behavior in the *n*-hexane−ethanol mixture. Introducing NBP into the mixture at lower pressures leads to a slight increase in the relative volatility of *n*-hexane to ethanol. However, as the amount of the NBP is increased from an E/F of 1 to 2 and 3 at 100.0 kPa, the relative volatility increases further, although the relative volatilities for E/F of 2 and 3 are similar. Furthermore, the relative volatility comparison of NBP and NMP reveals that NBP at E/F = 1 and 50.0 kPa, and E/F = 2 and 3 at 100.0 kPa, demonstrates a comparable performance to NMP at E/F = 1 and 100.0 kPa. These results emphasize the potential of NBP as a greener alternative entrainer to NMP for more sustainable and green extractive distillation in the separation of *n*-hexane and ethanol.

The VLE data were regressed by using the NRTL model. The regression results closely fit the experimental VLE data. Therefore, the optimum binary interaction parameters can be obtained. To represent an industrial-scale separation, this NRTL model and its optimum binary interaction parameters can be utilized to design an effective extractive distillation process for separating the *n*-hexane−ethanol mixture using the greener entrainer NBP. Future work will focus on simulating the extractive distillation process for the *n*-hexane−ethanol mixture using NBP and NMP as entrainers to evaluate the performance of both solvents under realistic column conditions.

■ ASSOCIATED CONTENT

Supporting Information

The Supporting Information is available free of charge at https://pubs.acs.org/doi/10.1021/acs.jced.5c00445.

Comparison of the x_1−y_1 diagram for the binary mixture *n*-hexane and ethanol between this work and the literature; comparison of experimental and literature vapor pressure for pure *n*-hexane and ethanol; comparison of experimental and literature VLE data for the *n*-hexane and NMP mixture; residual distribution of $\ln(\gamma_1/\gamma_2)$; residual plots for liquid and vapor compositions, and temperature; experimental vapor pressure data for pure *n*-hexane and ethanol; values of ΔP and Δy; and calculations of uncertainty (PDF)

■ AUTHOR INFORMATION

Corresponding Author

Dhoni Hartanto − *Department of Chemical Engineering, Delft University of Technology, Delft 2629 HZ, The Netherlands; Department of Chemical Engineering, Faculty of Engineering, Universitas Negeri Semarang, Semarang 50229, Indonesia;* orcid.org/0000-0003-4127-5361; Email: dhoni.hartanto@mail.unnes.ac.id

Authors

Boelo Schuur − *Sustainable Process Technology, Faculty of Science and Technology, University of Twente, Enschede 7500 AE, The Netherlands;* orcid.org/0000-0001-5169-4311

Anton A. Kiss − *Department of Chemical Engineering, Delft University of Technology, Delft 2629 HZ, The Netherlands*

André B. de Haan − *Department of Chemical Engineering, Delft University of Technology, Delft 2629 HZ, The Netherlands*

Complete contact information is available at: https://pubs.acs.org/10.1021/acs.jced.5c00445

Author Contributions

D.H.: Conceptualization, experimental works and analysis, data curation, and writing—original draft. B.S.: Supervision, conceptualization, methodology, and resources. A.A.K.: Supervision, conceptualization, methodology, project administration, writing—review and editing. A.B.d.H.: Supervision, conceptualization, funding acquisition, project administration, and writing—review and editing.

Notes

The authors declare no competing financial interest.

■ ACKNOWLEDGMENTS

This work was financially supported by a Ph.D. Scholarship awarded to Dhoni Hartanto, funded by the Indonesia Endowment Fund for Education (LPDP) under the Ministry of Finance of the Republic of Indonesia, with grant number SKPB-1597/LPDP/LPDP.3/2024. The authors sincerely acknowledge this financial support.

■ REFERENCES

(1) Chavez Velasco, J. A.; Tawarmalani, M.; Agrawal, R. Systematic Analysis Reveals Thermal Separations Are Not Necessarily Most Energy Intensive. *Joule* **2021**, *5* (2), 330−343.

(2) de Haan, A. B.; Eral, H. B.; Schuur, B. *Industrial Separation Processes*; De Gruyter, 2025.

(3) Hadj-Kali, M. K.; Hizaddin, H. F.; Wazeer, I.; El blidi, L.; Mulyono, S.; Hashim, M. A. Liquid-Liquid Separation of Azeotropic Mixtures of Ethanol/Alkanes Using Deep Eutectic Solvents: COSMO-RS Prediction and Experimental Validation. *Fluid Phase Equilib.* **2017**, *448*, 105−115.

(4) Muhammed, N. S.; Gbadamosi, A. O.; Epelle, E. I.; Abdulrasheed, A. A.; Haq, B.; Patil, S.; Al-Shehri, D.; Kamal, M. S. Hydrogen Production, Transportation, Utilization, and Storage: Recent Advances towards Sustainable Energy. *J. Energy Storage* **2023**, *73*, No. 109207.

(5) Kang, J.; He, S.; Zhou, W.; Shen, Z.; Li, Y.; Chen, M.; Zhang, Q.; Wang, Y. Single-Pass Transformation of Syngas into Ethanol with High Selectivity by Triple Tandem Catalysis. *Nat. Commun.* **2020**, *11* (1), No. 827.

(6) Speight, J. G. Hydrocarbons from Synthesis Gas. In *Handbook of Industrial Hydrocarbon Processes*, 2nd ed.; Speight, J. G., Ed.; Gulf Professional Publishing: Boston, 2020; Chapter 8, pp 343−386.

(7) Sbihi, H. M.; Nehdi, I. A.; Mokbli, S.; Romdhani-Younes, M.; Al-Resayes, S. I. Hexane and Ethanol Extracted Seed Oils and Leaf Essential Compositions from Two Castor Plant (*Ricinus communis* L.) Varieties. *Ind. Crops Prod.* **2018**, *122*, 174−181.

(8) Kiss, A. A.; Lange, J.-P.; Schuur, B.; Brilman, D. W. F.; van der Ham, A. G. J.; Kersten, S. R. A. Separation Technology−Making a Difference in Biorefineries. *Biomass Bioenergy* **2016**, *95*, 296−309.

(9) Kooijman, H. A.; Sorensen, E. Recent Advances and Future Perspectives on More Sustainable and Energy Efficient Distillation Processes. *Chem. Eng. Res. Des.* **2022**, *188*, 473−482.

(10) Kiss, A. A.Design, Control and Economics of Distillation. *Advanced Distillation Technologies*; John Wiley & Sons, Inc., 2013; pp 37−65.
(11) Sherwood, J.; Farmer, T. J.; Clark, J. H. Catalyst: Possible Consequences of the N-Methyl Pyrrolidone REACH Restriction. *Chem* **2018**, *4* (9), 2010−2012.
(12) Kirman, C. R.; Sonawane, B. R.; Seed, J. G.; Azu, N. O.; Barranco, W. T.; Hamilton, W. R.; Stedeford, T. J.; Hays, S. M. An Evaluation of Reproductive Toxicity Studies and Data Interpretation of N-Methylpyrrolidone for Risk Assessment: An Expert Panel Review. *Regul. Toxicol. Pharmacol.* **2023**, *138*, No. 105337.
(13) Sharma, A.; Lee, B.-S.; Shin, H. Y. Assessing Suitability of Glycerol-Derived Green Solvent for the Separation of n-Hexane + Ethanol Azeotropic Mixture, Accompanied by VLE Studies Using Machine Learning. *J. Mol. Liq.* **2025**, *423*, No. 127003.
(14) Neubauer, M.; Wallek, T.; Lux, S. Deep Eutectic Solvents as Entrainers in Extractive Distillation − A Review. *Chem. Eng. Res. Des.* **2022**, *184*, 402−418.
(15) Hartanto, D.; Schuur, B.; Kiss, A. A.; de Haan, A. B. In *Effective Selection of Green Organics and Natural Deep Eutectic Solvents as Advanced Entrainers by COSMO-RS and Group Contributions Methods for Enhanced Design of Extractive Distillation*, 34th European Symposium on Computer Aided Process Engineering/15th International Symposium on Process Systems Engineering; Manenti, F.; Reklaitis, G. V., Eds.; Elsevier, 2024; Vol. *53*, pp 1387−1392.
(16) Wang, W.; Wang, Y.; Lu, W.; Zhao, W.; Zhu, Z.; Cui, P.; Li, X.; Song, X. Experimental and Mechanism Study of Separation of Ethanol-Ethyl Tert-Butyl Ether with Deep Eutectic Solvents Based on Molecular Simulation. *Sep. Purif. Technol.* **2025**, *359*, No. 130587.
(17) Rahayu, S. D.; Altway, S.; Tiwikrama, A. H.; Kuswandi, K. Isobaric Vapor−Liquid Equilibria for Separation of the n-Propanol and Water Azeotropic System with the Addition of a Choline Chloride−Ethylene Glycol-Based Deep Eutectic Solvent as an Entrainer. *J. Chem. Eng. Data* **2025**, *70* (1), 416−426.
(18) Peng, Y.; Shen, Y.; Niu, J.; Han, X. Separation of Azeotropic Mixture Using a Novel Hybrid Entrainer Based on Deep Eutectic Solvents. *Fluid Phase Equilib.* **2025**, *592*, No. 114326.
(19) Hartanto, D.; Gupta, B. S.; Taha, M.; Lee, M. J. Isobaric Vapour-Liquid Equilibrium of (Tert-Butanol + Water) System with Biological Buffer TRIS at 101.3 KPa. *J. Chem. Thermodyn.* **2016**, *98*, 159−164.
(20) Iftakher, A.; Leonard, T.; Hasan, M. M. F. Integrating Different Fidelity Models for Process Optimization: A Case of Equilibrium and Rate-Based Extractive Distillation Using Ionic Liquids. *Comput. Chem. Eng.* **2025**, *192*, No. 108890.
(21) Zhang, J.; Pan, C.; Di, S.; Huang, Q.; Li, J.; Wang, Z.; Yang, Y.; Wang, N.; Chang, K.; Kong, L.; Fan, W.; Zhang, Z.; Jiang, S.; Hu, Y.; Liu, Z. Molecular Insights and Process Integration for Efficient Separation of Methanol/Methyl Ethyl Ketone by Ionic Liquid Extractive Distillation. *ACS Sustainable Chem. Eng.* **2025**, *13* (15), 5557−5568.
(22) Dong, Y.; Xu, F.; Xia, Y.; Yang, Q. Efficient Separation of Methanol, Acetonitrile, and Benzene Ternary Azeotropic Mixture Using Ionic Liquid in Extractive Distillation. *Sep. Purif. Technol.* **2025**, *360*, No. 131018.
(23) Yue, K.; Lu, J.; Chen, P.; Gu, S.; Zhou, G. Vapor−Liquid Equilibrium for Acetonitrile + Ethanol with Imidazole-Based Ionic Liquids as Entrainers at 101.3 KPa. *J. Chem. Eng. Data* **2024**, *69* (4), 1645−1654.
(24) Xing, Y.; Cui, X.; Xu, S.; Feng, T.; Zhang, X.; He, J.; Wang, J. Isobaric Vapor−Liquid Equilibrium for Methyl Acetate + Methanol with Double Salt Ionic Liquid [EMIM][Cl]0.5[DCA]0.5 as Entrainer at 101.3 KPa. *Fluid Phase Equilib.* **2021**, *541*, No. 113086.
(25) Pavlíček, J.; Bogdanić, G.; Wichterle, I. Azeotropic Behavior of the 2-Propanol + Water + 1-Ethyl-3-Methylimidazolium Bis-(Trifluoromethylsulfonyl)Imide System. *Fluid Phase Equilib.* **2023**, *563*, No. 113582.
(26) Brouwer, T.; Schuur, B. Biobased Entrainer Screening for Extractive Distillation of Acetone and Diisopropyl Ether. *Sep. Purif. Technol.* **2021**, *270*, No. 118749.
(27) Hartanto, D.; Schuur, B.; Schuttevaer, T.; Kiss, A. A.; de Haan, A. B. Isobaric Vapor−Liquid Equilibrium of Methylcyclohexane + Toluene with Gamma-Valerolactone as a Biobased Entrainer and 1-Methylpyrrolidin-2-One as a Conventional Entrainer. *J. Chem. Eng. Data* **2025**, *70* (3), 1339−1351.
(28) Brouwer, T.; Schuur, B. Bio-Based Solvents as Entrainers for Extractive Distillation in Aromatic/Aliphatic and Olefin/Paraffin Separation. *Green Chem.* **2020**, *22* (16), 5369−5375.
(29) Zhao, W.; Wu, Q.; Yang, L.; Wang, Z.; Xu, Y.; Zhu, Z.; Cui, P.; Wang, Y. Process Design, Optimization and Intensification for the Efficient Purification of the Green Solvent Cyclopentyl Methyl Ether. *Sep. Purif. Technol.* **2025**, *357*, No. 130049.
(30) Wang, Q.; Dai, P.; Yang, A.; Shen, W.; Zhang, J. Deep Learning-Driven Green Solvent Design and Process Intensification towards Isopropyl Alcohol-Water Azeotrope System. *Sep. Purif. Technol.* **2025**, *360*, No. 131103.
(31) Gomes, J. P.; Silva, R.; Nunes, C. P.; Barbosa, D. Towards Sustainable Industrial Processes: A Preselection Method for Screening Green Solvents in the 1,3-Butadiene Extractive Distillation Process. *Sustainability* **2025**, *17*, No. 3285.
(32) Ma, Y.; Hu, Z.; Yang, L.; Zhang, L.; Liu, S.; Zhang, Z.; Xu, D.; Gao, J.; Wang, Y. Extractive Distillation Separation of Isopropanol - Isopropyl Acetate Azeotrope: Vapor-Liquid Equilibrium Measurement and Process Optimization. *J. Chem. Thermodyn.* **2025**, *205*, No. 107460.
(33) Zhang, Y.; Wang, Z.; Xu, X.; Gao, J.; Xu, D.; Zhang, L.; Wang, Y. Entrainers Selection and Vapour-Liquid Equilibrium Measurements for Separating Azeotropic Mixtures (Ethanol + n-Hexane/Cyclohexane) by Extractive Distillation. *J. Chem. Thermodyn.* **2020**, *144*, No. 106070.
(34) Gonzalez, E.; Ortega, J. Densities and Isobaric Vapor-Liquid Equilibria of Butyl Esters (Methanoate to Butanoate) with Ethanol at 101.32 KPa. *J. Chem. Eng. Data* **1995**, *40* (6), 1178−1183.
(35) Wang, Y.; Hu, R.; Liu, W.; Zhu, Z.; Wang, Y.; Yang, J.; Qi, J.; Cui, P. Separation of Ethanol/n-Hexane Azeotrope by Imidazolium Ionic Liquids: Experimental Study and Mechanism Analysis. *Sep. Purif. Technol.* **2025**, *357*, No. 130063.
(36) Sander, A.; Petračić, A.; Rogošić, M.; Župan, M.; Frljak, L.; Cvetnić, M. Feasibility of Different Methods for Separating N-Hexane and Ethanol. *Separations* **2024**, *11*, No. 151.
(37) Wang, Y.; Xu, H.; Yang, Q.; Wang, W.; Li, H.; Wang, Y.; Zhu, Z.; Li, X.; Song, X.; Cui, P. A Novel Intermediate Heat Exchange Intensified Extractive Pressure-Swing Distillation Process for Efficiently Separating n-Hexane-Tetrahydrofuran-Ethanol. *Chem. Eng. Sci.* **2024**, *300*, No. 120593.
(38) European Chemical Agency. 1-Butylpyrrolidin-2-one, 2024. https://echa.europa.eu/registration-dossier/-/registered-dossier/10579 (accessed Aug 27, 2024).
(39) AICIS. Australian Industrial Chemicals Introduction Scheme (AICIS), Public Report, 2-Pyrrolidinone, 1-Butyl-; STD/1698, 2020. https://www.industrialchemicals.gov.au/sites/default/files/STD1698publicreport%5B780KB%5D.pdf.
(40) SCCS. Opinion on *N*-Methyl-2-pyrrolidone (NMP); SCCS/1413/11, 2011. https://ec.europa.eu/health/scientific_committees/consumer_safety/docs/sccs_o_050.pdf.
(41) Jiang, X.; Yong, W. F.; Gao, J.; Shao, D.-D.; Sun, S.-P. Understanding the Role of Substrates on Thin Film Composite Membranes: A Green Solvent Approach with TamiSolve® NxG. *J. Membr. Sci.* **2021**, *635*, No. 119530.
(42) Buken, O.; Mancini, K.; Sarkar, A. A Sustainable Approach to Cathode Delamination Using a Green Solvent. *RSC Adv.* **2021**, *11* (44), 27356−27368.
(43) Eastman. TamiSolve NxG, 2024. https://www.eastman.com/Pages/ProductHome.aspx?product=71103844&pn=TamiSolve+NxG (accessed Nov 11, 2024).

https://doi.org/10.1021/acs.jced.5c00445
J. Chem. Eng. Data 2025, 70, 4091−4104

(44) Eastman. *SDS TamiSolve® NxG-PS No. 150000112709*; Kingsport: Tennessee, United States, 2020.
(45) Palczewska-Tulińska, M.; Oracz, P. Vapor Pressures of 1-Methyl-2-Pyrrolidone, 1-Methyl-Azepan-2-One, and 1,2-Epoxy-3-Chloropropane. *J. Chem. Eng. Data* **2007**, *52* (6), 2468−2471.
(46) Li, N.; Han, X.; Lv, H.; Jin, Y.; Yu, J. Biodegradation of N-Methyl-2-Pyrrolidone (NMP) in Wastewater: A Review of Current Knowledge and Future Perspectives. *J. Cleaner Prod.* **2025**, *486*, No. 144452.
(47) European Chemical Agency. 1-Methyl-2-pyrrolidone, 2025. https://www.echa.europa.eu/substance-information/-/substanceinfo/100.011.662 (accessed Aug 04, 2025).
(48) Tian, X.; Wang, R.; Wang, H.; Li, C.; Liu, J. Energy-Saving Extractive Distillation Processes Design and Optimization for the Separation of Ethyl Acetate and n-Heptane Azeotrope. *Fuel* **2025**, *379*, No. 132974.
(49) Zhang, J.; Pan, C.; Ren, C.; Li, C.; Di, S.; Jiang, S.; Huang, Q.; Gao, N.; Wang, N.; Chang, K.; Kong, L.; Wang, Z.; Hu, Y.; Liu, Z.; Guo, X. Exploration of Energy-Saving Processes for the Separation of Tetrahydrofuran/Methanol/Water: From Separation Mechanism to Experimental Validation. *Fuel* **2025**, *388*, No. 134498.
(50) Zhang, R.; Xu, Z.; Li, J.; Pan, J.; Wang, H.; Dai, T.; Ye, Q. Sustainable Process Design and Multiobjective Optimization for Separation of N-Heptane/Tert-Butyl Acetate by Extractive Distillation: From Separation Mechanism to Experimental. *Ind. Eng. Chem. Res.* **2025**, *64* (12), 6676−6691.
(51) Van Ness, H. C. Thermodynamics in the Treatment of Vapor/Liquid Equilibrium (VLE) Data. *Pure Appl. Chem.* **1995**, *67* (6), 859−872.
(52) Renon, H.; Prausnitz, J. Local Compositions in Thermodynamic Excess Functions for Liquid Mixtures. *AIChE J.* **1968**, *14* (1), 135−144.
(53) Dias, T. P. V. B.; Fonseca, L. A. A. P.; Ruiz, M. C.; Batista, F. R. M.; Batista, E. A. C.; Meirelles, A. J. A. Vapor−Liquid Equilibrium of Mixtures Containing the Following Higher Alcohols: 2-Propanol, 2-Methyl-1-Propanol, and 3-Methyl-1-Butanol. *J. Chem. Eng. Data* **2014**, *59* (3), 659−665.
(54) Keestra, H.; Brouwer, T.; Schuur, B.; Lange, J.-P. Entrainer Selection for the Extractive Distillation of Acrylic Acid and Propionic Acid. *Chem. Eng. Res. Des.* **2023**, *192*, 653−663.
(55) Taylor, B. N.; Kuyatt, C. E. *Guidelines for Evaluating and Expressing the Uncertainty of NIST Measurement Results*. NIST Technical Note 1297; NIST, 1994.
(56) Working Group 1 of the Joint Committee for Guides in Metrology (JCGM/WG 1). *Evaluation of Measurement Data—Guide to the Expression of Uncertainty in Measurement*; International Organization for Standardization: Geneva, 2008; Vol. *50*, p 134.
(57) Sinor, J. E.; Weber, J. H. Vapor-Liquid Equilibria at Atmospheric Pressure. Systems Containing Ethyl Alcohol, n-Hexane, Benzene, and Methylcyclopentane. *J. Chem. Eng. Data* **1960**, *5* (3), 243−247.
(58) Ortega, J.; Espiau, F. A New Correlation Method for Vapor−Liquid Equilibria and Excess Enthalpies for Nonideal Solutions Using a Genetic Algorithm. Application to Ethanol + an n-Alkane Mixtures. *Ind. Eng. Chem. Res.* **2003**, *42* (20), 4978−4992.
(59) Willingham, C.; Taylor, W. J.; Pignocco, J. M.; Rossini, F. D. Vapor Pressures and Boiling Points of Some Paraffin, Alkylcyclopentane, Alkylcyclohexane, and Alkylbenzene Hydrocarbons. *J. Res. Natl. Bur. Stand.* **1945**, *35* (3), 219−244.
(60) Kretschmer, C. B.; Wiebe, R. Liquid-Vapor Equilibrium of Ethanol–Toluene Solutions. *J. Am. Chem. Soc.* **1949**, *71* (5), 1793−1797.
(61) Zhang, L.; Shen, D.; Zhang, Z.; Wu, X. Experimental Measurement and Modeling of Vapor−Liquid Equilibrium for the Ternary System Water + Acetonitrile + Ethylene Glycol. *J. Chem. Eng. Data* **2017**, *62* (5), 1725−1731.
(62) Zhang, Z.; Lv, M.; Huang, D.; Jia, P.; Sun, D.; Li, W. Isobaric Vapor−Liquid Equilibrium for the Extractive Distillation of Acetonitrile + Water Mixtures Using Dimethyl Sulfoxide at 101.3 KPa. *J. Chem. Eng. Data* **2013**, *58* (12), 3364−3369.
(63) Zhu, J.; Sun, Y.; Chen, Y.; Wu, N.; Shi, R.; Ren, Z.; Li, Q.; Zhao, H. Isobaric Vapor−Liquid Equilibrium Experiments of Methyl Propionate + Ethanol with Different Ionic Liquids at 101.3 KPa. *J. Chem. Eng. Data* **2025**, *70* (1), 427−438.
(64) Li, W.; Chen, X.; Yin, H.; Li, L.; Zhang, T. Isobaric Vapor−Liquid Equilibrium for 2-Butanone + Ethanol System Containing Different Ionic Liquids at 101.3 KPa. *J. Chem. Eng. Data* **2018**, *63* (2), 380−388.
(65) Li, W.; Li, L.; Zhang, L.; Li, H.; Zhang, T. Isobaric Vapor-Liquid Equilibrium for 2-Butanone + Ethanol + Phosphate-Based Ionic Liquids at 101.3 KPa. *Fluid Phase Equilib.* **2018**, *456*, 57−64.
(66) Blanco, B.; Beltrán, S.; Cabezas, J. L.; Coca, J. Phase Equilibria of Binary Systems Formed by Hydrocarbons from Petroleum Fractions and the Solvents N-Methylpyrrolidone and N,N-Dimethylformamide. 1. Isobaric Vapor−Liquid Equilibria. *J. Chem. Eng. Data* **1997**, *42* (5), 938−942.
(67) Li, M.; Yu, Y.; Zhang, L.; Li, J.; Song, Y. Isobaric Binary and Ternary Vapor−Liquid Equilibrium for the Mixture of n-Hexane, Methylcyclopentane and N-Methylpyrrolidone. *J. Solution Chem.* **2021**, *50* (9), 1258−1284.
(68) Li, F.; Li, M.; Guo, J.; Hu, X.; Zhu, J.; Li, Q.; Zhao, H. Isobaric Vapor−Liquid Equilibrium Experiment of N-Propanol and N-Propyl Acetate at 101.3 KPa. *J. Chem. Eng. Data* **2023**, *68* (2), 358−365.
(69) Cao, M.; Tian, H.; Li, M. Vapor−Liquid Equilibrium Data Determination and Model Correlation for 1-Octene + 1,4-Dioxane, 2-Octanol + 1,4-Dioxane, 1-Octene + Isophorone, and 2-Octanol + Isophorone Systems at 101.3 KPa. *J. Chem. Eng. Data* **2023**, *68* (9), 2275−2282.
(70) Lei, Z.; Arlt, W.; Wasserscheid, P. Selection of Entrainers in the 1-Hexene/n-Hexane System with a Limited Solubility. *Fluid Phase Equilib.* **2007**, *260* (1), 29−35.
(71) Zhang, Z.; Zhang, Z.; Dong, B.; Chen, J.; Xin, H.; Zhang, Q. Vapor-Liquid Equilibrium Experiment and Model Prediction for Separating Ethyl Propionate and Ethanol Using Ionic Liquids with Acetate Anion. *J. Mol. Liq.* **2020**, *318*, No. 113688.
(72) Yang, C.; Zeng, H.; Yin, X.; Ma, S.; Sun, F.; Li, Y.; Li, J. Measurement of (Vapor+liquid) Equilibrium for the Systems {methanol+dimethyl Carbonate} and {methanol+dimethyl Carbonate+tetramethylammonium Bicarbonate} at P = (34.43, 67.74)KPa. *J. Chem. Thermodyn.* **2012**, *53*, 158−166.
(73) He, S.; Fan, W.; Huang, H.; Gao, J.; Xu, D.; Ma, Y.; Zhang, L.; Wang, Y. Separation of the Azeotropic Mixture Methanol and Toluene Using Extractive Distillation: Entrainer Determination, Vapor−Liquid Equilibrium Measurement, and Modeling. *ACS Omega* **2021**, *6* (50), 34736−34743.
(74) Britt, H. I.; Luecke, R. H. The Estimation of Parameters in Nonlinear, Implicit Models. *Technometrics* **1973**, *15* (2), 233−247.

https://doi.org/10.1021/acs.jced.5c00445
J. Chem. Eng. Data 2025, 70, 4091−4104